Active lateral force feedback using resonant traveling waves

Cai, Zhaochong; Wiertlewski, Michael

DOI
10.1109/TOH.2023.3276590

Publication date
2023

Document Version
Final published version

Published in
IEEE Transactions on Haptics

Ultraloop: Active Lateral Force Feedback Using Resonant Traveling Waves

Zhaochong Cai and Michaël Wiertlewski, *Member, IEEE*

***Abstract*—The sensation of touching virtual texture and shape can be provided to a touchscreen user by varying the friction force. Despite the saliency of the sensation, this modulated frictional force is purely passive and strictly opposes finger movement. Therefore, it is only possible to create forces along the direction of movement and this technology cannot stimulate a static fingertip or provide forces that are orthogonal to the direction of movement. The lack of orthogonal force limits the guidance to a target in an arbitrary direction and there is a need for active lateral forces to give directional cues to the fingertip. Here, we introduce a surface haptic interface that uses ultrasonic traveling waves to create an active lateral force on bare fingertips. The device is built around a ring shape cavity where two degenerate resonant modes around 40 kHz are excited with 90° phase shift. The interface provides active forces up to 0.3 N to a static bare finger uniformly over a 140×30 mm^2 surface. We report the model and design of the acoustic cavity, force measurements, and an application to create a key-click sensation. This work demonstrates a promising method for uniformly producing large lateral forces on a touch surface.**

***Index Terms*—Surface haptics, lateral force feedback, active force, ultrasonic vibration, traveling waves.**

I. Introduction

TOUCHSCREENS and capacitive buttons offer designers the flexibility to program human-machine interfaces but deprive users of tactile feedback typically found in mechanical buttons. Without feedback, the interaction becomes cognitively demanding and requires constant visual attention. Surface haptic interfaces can restore tactile feedback by creating rich and tangible interfaces. Among these technologies, friction modulation is a popular method to stimulate users' sense of touch. It operates by changing the force applied to a sliding fingertip. Friction can be modulated either by ultrasonic lubrication, which uses acoustic levitation to reduce friction [1], [2], [3], or electroadhesion which relies on electrostatic attraction to increase friction [4], [5], [6]. Both methods are able to render a wide range of effects, from textures, shapes, to viscosity by modulating the magnitude of the friction force as a function of the user motion [4], [7], [8].

Manuscript received 2 December 2022; revised 13 March 2023; accepted 4 May 2023. Date of publication 18 May 2023; date of current version 19 December 2023. This paper was recommended for publication by Associate Editor M. Konyo and Editor-in-Chief S. Choi upon evaluation of the reviewers' comments. The work of Zhaochong Cai was supported by China Scholarship Council under Grant 202006320048. *(Corresponding author: Zhaochong Cai.)*

The authors are with the Cognitive Robotics (CoR) Department, Faculty 3mE, Delft University of Technology, 2628 CD Delft, The Netherlands (e-mail: z.cai-1@tudelft.nl; m.wiertlewski@tudelft.nl).

This article has supplementary downloadable material available at https://doi.org/10.1109/TOH.2023.3276590, provided by the authors.

Digital Object Identifier 10.1109/TOH.2023.3276590

However, frictional forces are essentially passive forces that only resist finger motion instead of actively pushing fingers. Because of this, modulating frictional force is only effective on a sliding finger and the force is oriented opposite to the movement direction. Although literature reported that a stationary finger can also perceive a sudden change in friction [9], the feedback is feint and it fails to provide directional cues. Applications such as guiding the finger or navigating through a curved channel, require an active lateral force.

One strategy to generate active lateral forces on a touchpad is to use asymmetric friction. Asymmetric friction devices synchronize in-plane oscillation and friction modulation either via ultrasonic vibration [10] or electroadhesion [11]. During part of one oscillation cycle, friction is set to high, while during the rest of the oscillation cycle, the friction is set to low, causing a non-zero asymmetric force profile during one full cycle. The lateral oscillation can be created with a voice coil [10] excited at low frequency and can reach a maximum lateral force of up to 450 mN [11]. However, these devices suffer from the audible noise produced by lateral oscillation. UltraShiver eliminated the audible noise by vibrating the plate in an ultrasonic regime [12]. However, this device operates with resonant mode and therefore has several nodal lines where the sensation is null. To circumvent this problem, a new device SwitchPad switches between the first and the second in-plane oscillation mode according to the finger position [13], achieving a 250 mN peak force.

The other principle that generates active lateral forces induces an elliptical motion of the surface. Elliptical motion can be achieved by exciting both the longitudinal and bending modes of a plate at the same frequency. Using this strategy, the LateralPad can produce active shear forces of ± 50 mN [14] and the 2MoTac can generate shear forces to simulate a button-click [15], [16]. However, matching the resonant frequency of the two modes requires a precise mechanical design and stable mechanical properties. Another approach to induce an elliptical motion at the surface is to leverage flexural traveling waves. This method is the driving mechanism behind commercial ultrasonic motors [17]. Biet et al. first reported that placing the finger on an ultrasonic motor creates a strong propelling sensation [18]. Such motors can be used to create button clicks [19]. Despite its compelling force feedback, ultrasonic motors are not specifically designed for haptic application and their circular shape makes them ill-suited as tactile interfaces which are typically rectangular. Ghenna et al. proposed a device that can generate traveling waves in a straight beam actuated by two Langevin transducers [20].

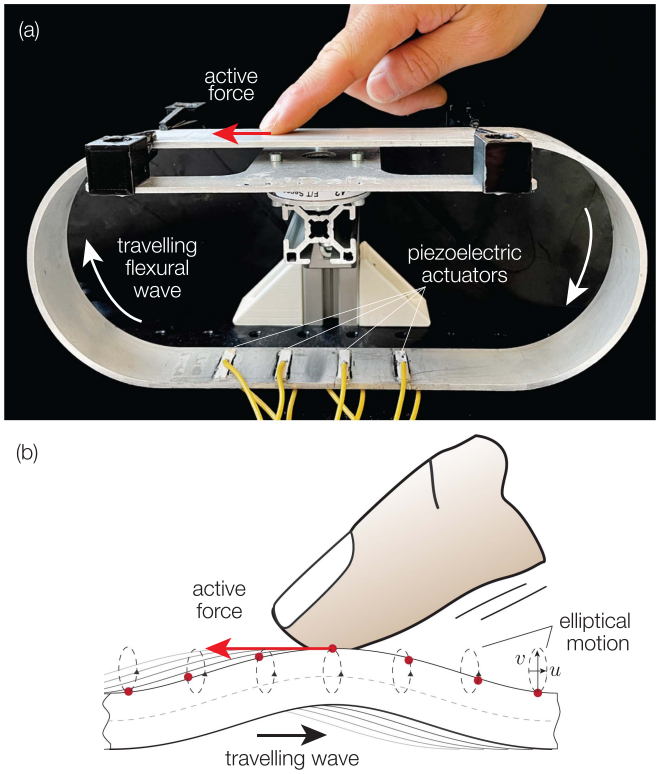

Fig. 1. (a) Ultraloop is a traveling wave surface haptic interface. Piezoelectric actuators excite two degenerate modes of the structure that superimpose as a traveling wave. (b) The traveling wave creates an elliptical motion of the surface points which actively pushes the fingertip.

However, the design does not use resonance and achieves modest active forces of 100 mN despite powerful actuators.

In this paper, we report a novel haptic device, the Ultraloop (Fig. 1(a)), that can generate active lateral forces up to 300 mN using resonant traveling waves. The active forces are uniformly produced on a rectangular surface (140 × 30 mm) which is large enough for comfortable interaction. The ring-shaped structure has no acoustic boundary and therefore is ideal for efficiently propagating traveling waves and creating sufficiently strong active forces to create numerous applications. A keyclick simulation is demonstrated, as a proof of concept, to show its capability to manipulate lateral forces temporally and spatially for various effects.

II. Design of a Traveling Wave Structure

A. Traveling Wave Excitation and Lateral Force Generation

Because of the wave reflection in the boundary, generating traveling waves in a finite beam comes with compromises. One strategy pioneered by Kuribayashi et al. [21], is to use two actuators: one to excite a traveling wave and the other to absorb it before it reflects on the boundary created by end of the beam. One key limitation of this approach is that because the wave is absorbed, the vibration can only achieve a modest displacement.

Producing larger displacement is possible by leveraging resonance. Our method uses the fact that two orthogonal resonant standing waves superimpose in a traveling wave if they are excited with a $\pm 90^\circ$ phase shift such that:

$$\sin(\omega t)\sin(kx) + \cos(\omega t)\cos(kx) = \cos(kx - \omega t) \tag{1}$$

where t is the time, x is the position, ω is the angular frequency and k is the wave number.

The superposition is achieved by exciting two successive flexural modes of the beam at the average frequency of each mode [20], [22]. However, because the frequency is in between two modes, the efficiency of the actuation is limited. A more efficient method to generate traveling waves is to superimpose two degenerate modes of a closed loop structure. These two degenerate modes have an identical resonant frequency, achieving higher efficiency. Examples include circular shape structures such as ultrasonic motors [17], ring-type resonator which already has been used in linear ultrasonic motors [23] and linear transportation system [24]. To generate traveling waves, our design relies on an oblong ring which provides a rectangular area that is convenient to interact with.

When traveling waves are propagating in the beam, the neutral line follows a transverse sinusoidal trajectory while the particles on the surface move along an elliptical locus due to an additional longitudinal movement. When an object, such as a finger, contacts the surface points, a relative displacement at the contact point leads to frictional force, pushing the object in the opposite direction than the wave propagation (Fig. 1(b)).

B. Orthogonal Degenerate Modes

The Ultraloop has a ring-type structure, comprising two straight beams of length L and two semicircular segments of radius R (Fig. 2(a)). For specific geometry, this type of structure has two orthogonal frequency-degenerate modes necessary to generate traveling waves. Here, we will briefly derive the solutions for the two degenerate modes. A comprehensive model of this resonator can be found in [25], [26].

1) Differential Equations and Boundary Conditions: The Ultraloop has a uniform width w and thickness h, with Young's modulus E and density ρ. By applying the Euler-Bernoulli beam theory and employing Hamilton's principle, we yield governing partial differential equations.

For the straight part,

$$-\rho A\frac{\partial^2 v_s}{\partial t^2} + \rho I\frac{\partial^2}{\partial t^2}\frac{\partial^2 v_s}{\partial x^2} - EI\frac{\partial^4 v_s}{\partial x^4} = 0 \tag{2}$$

where $A = wh$ is the area of the cross-section, $I = wh^3/12$ is the second moment of area, and $v_s(x,t)$ is the transverse displacement.

For the curved part,

$$\rho AR\left(\frac{\partial^4 u_c}{\partial\theta^2\partial t^2} - \frac{\partial^2 u_c}{\partial t^2}\right) + \frac{EI}{R^3}\left(\frac{\partial^6 u_c}{\partial\theta^6} + 2\frac{\partial^4 u_c}{\partial\theta^4} + \frac{\partial^2 u_c}{\partial\theta^2}\right) - \frac{\rho I}{R}\left(\frac{\partial^6 u_c}{\partial\theta^4\partial t^2} + 2\frac{\partial^4 u_c}{\partial\theta^2\partial t^2} + \frac{\partial^2 u_c}{\partial t^2}\right) = 0 \tag{3}$$

where $u_c(x,t)$ is the longitudinal displacement respectively.

We then consider the boundary conditions. Because of the continuity of the structure, the boundary where the straight and

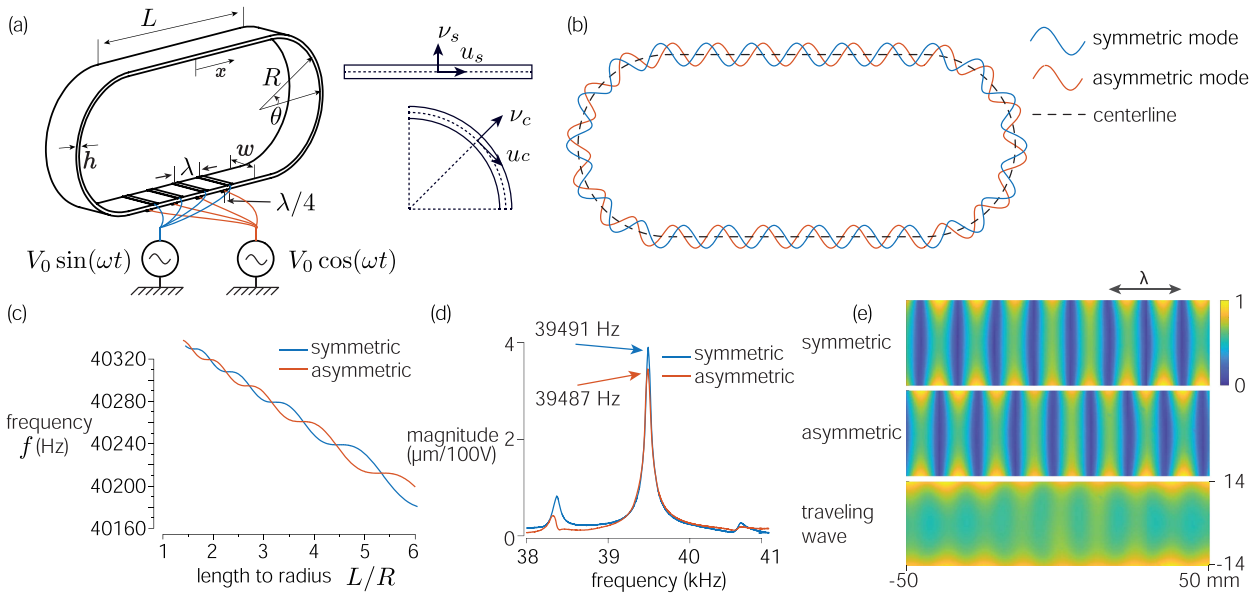

Fig. 2. (a) Schematic view of the Ultraloop. (b) Symmetric and asymmetric mode of the 24th order. (c) Natural frequency of the 24th modes for various length-to-radius ratios. (d) Experimental Bode plot of the two frequency-degenerate modes. (e) Mode shapes of symmetric mode, asymmetric mode and the resulting traveling wave are shown as normalized colormaps. The color at each grid corresponds to the vibration amplitude measured by a laser Doppler vibrometer. Note that the symmetric mode and asymmetric mode are orthogonal to each other.

curved parts connect must have the same displacements and rotations. Therefore, the boundary conditions can be described as:

$$v_s\left(\frac{L}{2},t\right) = v_c\left(-\frac{\pi}{2},t\right) \tag{4}$$

$$\frac{\partial v_s}{\partial x}\left(\frac{L}{2},t\right) = \frac{\partial v_c}{\partial s}\left(-\frac{\pi}{2},t\right) \tag{5}$$

2) Solutions: We use the method of separation of variables to decompose the solutions to a spatial part (i.e. the mode shape) with the variable x or θ, multiplied by a harmonic part along time with an angular frequency ω, i.e. $v_s(x,t) = V_s(x)\sin(\omega t)$ and $u_c(\theta,t) = U_c(\theta)\sin(\omega t)$. Note that here we only use u_c to represent the motion of the curved part due to an additional constraint between its transverse movement and its longitudinal movement, i.e. $v_c = -\partial u_c/\partial\theta$ if applying inextensionality condition.

Next, we will only consider the particular solutions of interest with the form of $\pm\sin$ and $\pm\cos$, which are flexural modes along the length of the Ultraloop. In this case, there are two solutions considering all the combinations:

- *Solution 1:* $\{V_s, U_c\} = \{A_s \cos k_s x, A_c \sin k_c\theta\}$ for symmetric mode and $\{V_s, U_c\} = \{A_s \sin k_s x, A_c \cos k_c\theta\}$ for asymmetric mode.
- *Solution 2:* $\{V_s, U_c\} = \{A_s \cos k_s x, A_c \cos k_c\theta\}$ for y-axis symmetric mode and $\{V_s, U_c\} = \{A_s \sin k_s x, A_c \sin k_c\theta\}$ for x-axis symmetric mode.

where k_s and k_c are the wave number in the straight part and the curved part respectively, A_s and A_c are the vibration amplitude in the straight part and the curved part respectively. We chose the 24th degenerate mode since its corresponding wavelength is of similar size to what is used in friction modulation ultrasonic devices and large enough to easily place piezoelectric actuators. The mode shape is shown in Fig. 2(b).

Substituting any of the above four modes into (2) and (3), the following two equations relating k_s and k_c are obtained:

$$k_s^4 - \alpha_s k_s^2\omega^2 - \gamma_s\omega^2 = 0 \tag{6}$$

where $\alpha_s = \rho/E$ and $\gamma_s = \rho A/EI$, and

$$\omega^2(\gamma_c k_c^4 - 2\gamma_c k_c^2 + \alpha_c k_c^2 + \alpha_c + \gamma_c) - k_c^6 + 2k_c^4 - k_c^2 = 0 \tag{7}$$

where $\alpha_c = \rho A R^4/EI$ and $\gamma_c = \rho R^2/E$.

Now we use the symmetric mode of Solution 1 as an example of how to derive the mode shapes. By substituting the solution into the boundary conditions (4) and (5), while remembering that $ds = Rd\theta$, we obtain

$$A_s \cos\left(k_s\frac{L}{2}\right) = -A_c k_c \cos\left(-k_c\frac{\pi}{2}\right) \tag{8}$$

$$-A_s k_s \sin\left(k_s\frac{L}{2}\right) = \frac{A_c k_c^2}{R}\sin\left(-k_c\frac{\pi}{2}\right) \tag{9}$$

We have now four equations (6), (7), (8) and (9) with four unknowns including k_s, k_c, ω, and a ratio $\Gamma = A_s/A_c k_c$. The values of the unknowns are therefore fully defined. However, the equations are transcendental, so we numerically solve this system of equations to find the solutions.

First, we express the ratio Γ in two ways derived from (8) and (9)

$$\Gamma_1 = \frac{-\cos(-k_c\frac{\pi}{2})}{\cos(k_s\frac{L}{2})} \quad \text{and} \quad \Gamma_2 = \frac{-k_c\sin(-k_c\frac{\pi}{2})}{Rk_s\sin(k_s\frac{L}{2})} \tag{10}$$

then define a cost function:

$$g = (\Gamma_1 - \Gamma_2)^2 \tag{11}$$

The cost function g has a single argument, k_c, since k_s can be expressed by k_c using (6) and (7). Note that g equals 0 only when $\Gamma_1 = \Gamma_2$, which are equivalent to the constraints given by (8) and (9). Therefore, solving these equations becomes a problem of finding k_c for which $g(k_c) = 0$.

We can compute g as a function of k_c, and each local minimum of g would corresponds to a symmetric mode of a given order. Similarly, for the other three types of mode shapes, i.e. asymmetric mode of Solution 1 and the two degenerate modes of Solution 2, solutions of k_c can be found by computing the local minimum of their corresponding cost function g. Notably, all the flexural modes with an even order are given by Solution 1, while all those with an odd order are given by Solution 2.

Another important feature of the two degenerate modes is that their natural frequencies are identical for specific length-to-radius L/R ratios. Fig. 2(c) shows the resonant frequency dependence on the length-to-radius ratio of the 24th symmetric and asymmetric modes. The two frequency curves coincide at discrete values, which are preferred for traveling wave generation.

In summary, resonant frequencies of any mode can be calculated numerically given a certain size of the Ultraloop. An iterative process can be used to achieve desired dimensions and resonances. Optimization of design parameters can be further investigated based on the model. Here we choose the following geometrical parameters for the Ultraloop: $L = 140$ mm, $R = 50$ mm, $h = 2.75$ mm and $w = 30$ mm. The device is made from aluminum 5052, with $E = 69$ GPa and $\rho = 2680$ kg/m^3. With these numbers, we calculated the natural frequencies of 24th degenerate modes to be 40287 Hz and 40294 Hz. In practice, the resonant frequencies coincided but their values are lower than the analytical model predicts probably due to the error from Euler-Bernoulli beam assumption, see Fig. 2(d). The actual mode shapes of 24th degenerate modes as well as their superposition under a 90° phase shift were measured with a laser Doppler vibrometer, see Fig. 2(e).

III. Implementation

A. Ultraloop Fabrication and Piezoelectric Actuators

We fabricated the Ultraloop by electrical discharge machining and polished its top surface to make it smooth to the touch. Eight piezoelectric actuators were glued on the bottom plate of the structure, with four on the upper surface to excite the symmetric mode and the other four on the lower surface to excite the asymmetric mode. The piezoelectric actuators on the lower surface are shifted by a quarter wavelength. These piezoelectric actuators are 25 mm long, 5 mm wide and 0.3 mm thick piezo ceramic plates (SMPL25W5T30311, Steiner & Martins Inc) glued with epoxy adhesive (DP490, 3 M). The piezoelectric patches are ≈5 times smaller than the wavelength. Each set of ceramics is placed on the antinode of each mode.

The two driving signals for the piezoelectric actuators are generated by a functional generator (AFG 1062, Tektronix) and amplified by two 20× amplifiers (PD200, PiezoDrive). The maximum amplitude was ±80 V. The amplitude and phase shift was controlled through Matlab.

Although the analytical model predicts resonant frequencies of the two degenerate modes, their actual values can shift. During experiments, we first identified the resonant frequencies with a vibrometer. The working frequency was set as the middle of two resonant frequencies.

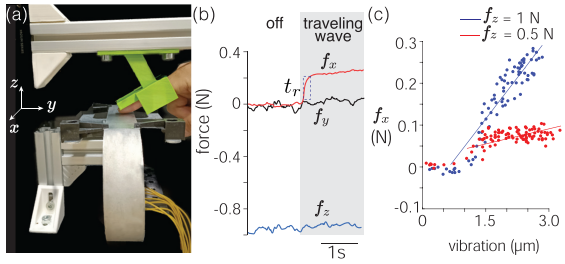

Fig. 3. Lateral force generation on a fixed finger. (a) Force measurement setup. The index finger is fixed by a supporting frame. (b) A typical trial where traveling waves produce a noticeable lateral force after a rise time of $t_r = 0.19$ s. (c) Influence of the vibration amplitude on the lateral force.

B. Vibration and Force Measurements

The ultrasonic vibration of the Ultraloop was measured by a Laser Doppler Vibrometer (OFV-503 and OFV-5000, Polytec). A laser beam was focused on the top surface and normal to this plane. Therefore the normal velocity of the oscillation of surface points on the Ultraloop was recorded. Displacement can be recovered by integrating the velocity. A force measurement setup was used to measure the lateral forces applied to the participant's finger, as shown in Fig. 3(a). The Ultraloop is supported by four 3d-print PLA fixtures at each corner of the upper straight part. These fixtures are mounted on a supporting plate, which stands on the top of the six-axis force sensor (Nano 43, ATI). The force data is acquired by a data acquisition card (USB 6351, National Instruments) at a sampling rate of 1 kHz.

The index finger of the participant was fixed by a supporting frame, with the finger pad facing the top surface of the Ultraloop. The supporting frame is attached to a manual linear stage on the z-axis. During each force measurement, the supporting frame, along with the finger was lowered down until the normal force reached ≈1 N.

IV. Results

A. Lateral Force Generation

Fig. 3(b) shows a typical trial of active lateral force generation on a fixed finger. When there was no vibration, forces on the lateral plane f_x and f_y remained almost zero. When traveling waves were generated on the Ultraloop by turning on both channels (39.5 kHz, 90° phase shift). Lateral force f_x experienced a rapid increase from 0 to roughly 0.22 N. Additionally, a static object placed on the Ultraloop surface can be moved smoothly (see supplementary video available in the online supplemental material.). The results show a significant lateral force generation on even a stationary object once traveling waves are present.

B. Lateral Force vs Vibration Amplitude

For large vibration amplitude, we would expect that the ellipsoidal movement of the surface be scaled and therefore the force would increase. We measured lateral forces f_x under

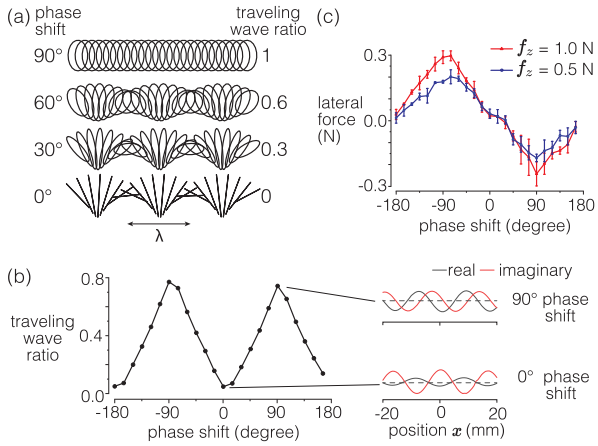

Fig. 4. Effect of the phase shift. (a) Theoretical result of surface point trajectories under different phase shifts between the two degenerate modes. The traveling wave ratio is defined as the ratio between the minimum amplitude to the maximum amplitude across the surface. (b) Measured traveling wave ratio for different phase shifts. The insets show the spatial distribution of the real and imaginary parts of the wave given by the Fourier transform. (c) Lateral force was measured under two normal forces: 1 N and 0.5 N. Force at each phase shift was measured 3 times on the same finger and averaged. The error bar shows the standard deviation.

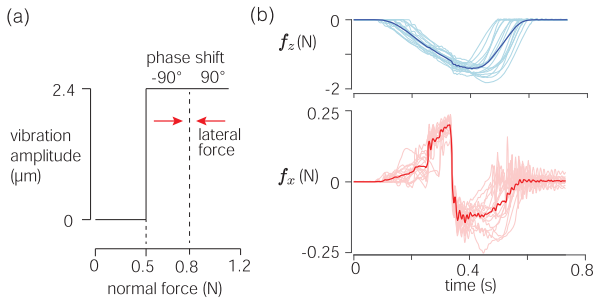

Fig. 5. (a) Control scheme to render a key-click illusion. Vibration is turned on when the normal force reaches 0.5 N. Phase shift switches from $-90°$ to $90°$ when the normal force rises to 0.8 N. The red arrows indicate the lateral force direction under different phase shifts. (b) Force measurement during pressing on the top surface of the Ultraloop with the index finger 16 times. The curves are aligned with the moment when the lateral force crosses the x-axis. Bold curves are the average of the 16 trials. The sudden reverse of the lateral force direction confirms a clear key-click event. Because of latency, the lateral force lags behind the normal force.

various amplitudes when normal force $f_z = 0.5$ N and 1.0 N and Fig. 3(c) shows a linear dependence of the lateral force on the vibration amplitude. The linear regression for $f_z = 1.0$ N leads to coefficient b = 0.13 N/μm. Our setup does not exceed ± 3 μm, but with more powerful piezoelectric actuators it might be possible to reach even larger lateral forces. In addition, under small vibration amplitude (less than ± 1.3 μm), the force appears weaker than the linear fit line. For vibration amplitude smaller than ± 1.0 μm, lateral force becomes insignificant compared to the measurement noise of our setup, suggesting that there is a minimum amplitude that needs to be reached to produce meaningful lateral forces.

The maximum vibration amplitude is ± 3 μm. Increasing amplitude might increase the force, but at the same time increase the potential for levitation, which might indicate that a plateau could be reached for higher vibration amplitude.

C. Effect of Arbitrary Phase Shifts

The quality of the traveling wave is strongly influenced by the correct superposition of the symmetric and asymmetric modes. To investigate this effect, we studied how the phase shift between the two modes influences the traveling wave generation. The superposition leads to a pure traveling wave only if the modes are shifted by $\pm 90°$. If the phase shift is $0°$ or $\pm 180°$, the waves superpose in a standing wave leading to squeeze film levitation. The pure traveling wave generates a uniform elliptical motion of the surface, however, nodal lines will appear if the phase shift is not perfectly $\pm 90°$. The effect of the phase shift on the surface motion is shown in Fig. 4(a). The ellipses tilt and shrink to straight lines as the phase shift changes from $90°$ to $0°$. For a $90°$ phase shift, the ellipses are identical along the surface and have the largest aspect ratio. For $0°$ phase shift, the trajectories are lines, which cannot cause any net lateral force during.

Fig. 4(b) shows the traveling wave ratio, measured with the vibrometer, which quantifies the uniformity of the wave magnitude across the length of the interface. A large traveling wave ratio corresponds to a high-purity traveling wave, where the real and imaginary parts of the wave are shifted by a quarter wavelength. The real and imaginary parts are found using the Fourier transform on the time domain displacement trace. Standing waves are found when the traveling wave ratio is close to zero and the real and imaginary are shifted by half a wavelength.

The lateral forces measured at these phase shifts follow a similar trend as the traveling wave ratio. Fig. 4(c) shows the force peaks at $-90°$ and $90°$ and attenuates to almost zero at 0 phase shift under both normal force cases (1 N and 0.5 N). Notably, the force reverses its direction when the phase shift is negative. Additionally, a lateral force under $f_z = 1$ N is higher than the force under $f_z = 0.5$ N.

D. Application: Key-Click Simulation

To demonstrate the potential application of this device, we implemented a button click, similar to [19]. The button click signal is a square wave where the traveling wave is turned on to the right ($-90°$ phase shift) when the normal force exceeds 0.5 N, and then to the left ($+90°$ phase shift) when the normal force exceeds 0.8 N, as shown in Fig. 5(a). With this control scheme, the finger experiences a sudden change in the shear force direction when the finger presses down.

We simulated several click events on the Ultraloop and recorded both the normal force and lateral force, which are presented in Fig. 5(b). Consistent with previous results, the lateral force first rises as the finger applies increasing pressure, then drops suddenly to a negative value when the phase shift reverses. The fast change in force direction produces a distinct confirmation of a successful click.

V. Conclusion

In this article, we report the development of a surface haptic device using resonant traveling waves, to generate a large active lateral force of up to 300 mN on static fingertips. The device has a simple loop structure that circulates acoustic energy, making it energy-efficient. The device does not have moving parts making

it suitable to be integrated into multimodal human-machine interfaces. The paper describes the theory that allows computing the optimal geometry and material suitable for any design. The force can be operated by tuning the phase shift and the amplitude of the traveling wave which opens the door for a host of haptic effects. By controlling the force as a function of the user's motion, we anticipate being able to render a virtual environment, such as potential wells or viscous environment, effectively creating a force-feedback device for fingertips.

Our future work will focus on reproducing virtual shapes by incorporating a finger position tracking. Psychophysical experiments will be implemented to evaluate the benefit of this interface when interacting with complex environments. In addition, we will miniaturize the design of Ultraloop and allow it to work in two-dimensional plane.

ACKNOWLEDGMENT

The authors would like to thank Shell for gifting the Laser Doppler vibrometer. The authors acknowledge the contribution of Hugo Maillard to early prototypes and thank David Abbink for inspiring discussions.

REFERENCES

[1] T. Watanabe and S. Fukui, "A method for controlling tactile sensation of surface roughness using ultrasonic vibration," in *Proc. IEEE Int. Conf. Robot. Automat.*, vol. 1, 1995, pp. 1134–1139.

[2] L. Winfield, J. Glassmire, J. E. Colgate, and M. Peshkin, "T-PaD: Tactile pattern display through variable friction reduction," in *Proc. 2nd Joint EuroHaptics Conf. Symp. Haptic Interfaces Virtual Environ. Teleoperator Syst.*, 2007, pp. 421–426.

[3] M. Wiertlewski, F. R. Fenton, and J. E. Colgate, "Partial squeeze film levitation modulates fingertip friction," *Proc. Nat. Acad. Sci.*, vol. 113, no. 33, pp. 9210–9215, Aug. 2016.

[4] O. Bau, I. Poupyrev, A. Israr, and C. Harrison, "TeslaTouch: Electrovibration for touch surfaces," in *Proc. 23nd Annu. ACM Symp. User Interface Softw. Technol.*, 2010, pp. 283–292.

[5] C. D. Shultz, M. A. Peshkin, and J. E. Colgate, "Surface haptics via electroadhesion: Expanding electrovibration with Johnsen and Rahbek," in *Proc. IEEE World Haptics Conf.*, 2015, pp. 57–62.

[6] M. Ayyildiz, M. Scaraggi, O. Sirin, C. Basdogan, and B. N. J. Persson, "Contact mechanics between the human finger and a touchscreen under electroadhesion," *Proc. Nat. Acad. Sci.*, vol. 115, no. 50, pp. 12668–12673, Dec. 2018.

[7] M. Wiertlewski, D. Leonardis, D. J. Meyer, M. A. Peshkin, and J. E. Colgate, "A High-Fidelity Surface-Haptic Device for Texture Rendering on Bare Finger," in *Proc. Int. Conf. Hum. Haptic Sens. Touch Enabled Comput. Appl.*, 2014, pp. 241–248.

[8] V. Levesque et al., "Enhancing physicality in touch interaction with programmable friction," in *Proc. SIGCHI Conf. Hum. Factors Comput. Syst.*, 2011, pp. 2481–2490.

[9] J. Monnoyer, E. Diaz, C. Bourdin, and M. Wiertlewski, "Ultrasonic friction modulation while pressing induces a tactile feedback," in *Int. Conf. Hum. Haptic Sens. Touch Enabled Comput. Appl.*, 2016, pp. 171–179.

[10] E. C. Chubb, J. E. Colgate, and M. A. Peshkin, "ShiverPaD: A glass haptic surface that produces shear force on a bare finger," *IEEE Trans. Haptics*, vol. 3, no. 3, pp. 189–198, Jul.–Sep. 2010.

[11] J. Mullenbach, M. Peshkin, and J. E. Colgate, "eShiver: Lateral force feedback on fingertips through oscillatory motion of an electroadhesive surface," *IEEE Trans. Haptics*, vol. 10, no. 3, pp. 358–370, Jul.–Sep. 2017.

[12] H. Xu, M. A. Peshkin, and J. E. Colgate, "UltraShiver: Lateral force feedback on a bare fingertip via ultrasonic oscillation and electroadhesion," *IEEE Trans. Haptics*, vol. 12, no. 4, pp. 497–507, Oct.–Dec. 2019.

[13] H. Xu, M. A. Peshkin, and J. E. Colgate, "SwitchPaD: Active lateral force feedback over a large area based on switching resonant modes," in *Proc. Int. Conf. Hum. Haptic Sens. Touch Enabled Comput. Appl.*, 2020, pp. 217–225.

[14] X. Dai, J. E. Colgate, and M. A. Peshkin, "LateralPaD: A surface-haptic device that produces lateral forces on a bare finger," in *Proc. IEEE Haptics Symp.*, 2012, pp. 7–14.

[15] P. Garcia, F. Giraud, B. Lemaire-Semail, M. Rupin, and M. Amberg, "2MoTac: Simulation of Button Click by Superposition of Two Ultrasonic Plate Waves," in *Proc. Int. Conf. Hum. Haptic Sens. Touch Enabled Comput. Appl.*, 2020, pp. 343–352.

[16] P. Garcia, F. Giraud, B. Lemaire-Semail, M. Rupin, and A. Kaci, "Control of an ultrasonic haptic interface for button simulation," *Sensors Actuators A: Phys.*, vol. 342, Aug. 2022, Art. no. 113624.

[17] Shinsei Corporation, "Ultrasonic wave motor: The first actuator incorporating ceramic technology," in *Piezoelectricity (Key Papers in Physics; No.5)*, C. Z. Rosen, B. V. Hiremath, and R. Newnham, Eds. New York, NY, USA: America Inst. Phys., 1992, pp. 381–383.

[18] M. Biet, F. Giraud, F. Martinot, and B. Semail, "A piezoelectric tactile display using travelling lamb wave," in *Proc. EuroHaptics Conf.*, 2006, pp. 567–570.

[19] D. Gueorguiev, A. Kaci, M. Amberg, F. Giraud, and B. Lemaire-Semail, "Travelling ultrasonic wave enhances keyclick sensation," in *Proc. Int. Conf. Hum. Haptic Sens. Touch Enabled Comput. Appl.*, 2018, pp. 302–312.

[20] S. Ghenna, E. Vezzoli, C. Giraud-Audine, F. Giraud, M. Amberg, and B. Lemaire-Semail, "Enhancing variable friction tactile display using an ultrasonic travelling wave," *IEEE Trans. Haptics*, vol. 10, no. 2, pp. 296–301, Apr.–Jun. 2017.

[21] M. Kuribayashi, S. Ueha, and E. Mori, "Excitation conditions of flexural traveling waves for a reversible ultrasonic linear motor," *J. Acoust. Soc. Amer.*, vol. 77, no. 4, pp. 1431–1435, Apr. 1985.

[22] B.-G. Loh and P. Ro, "An object transport system using flexural ultrasonic progressive waves generated by two-mode excitation," *IEEE Trans. Ultrasonics, Ferroelect., Freq. Control*, vol. 47, no. 4, pp. 994–999, Jul. 2000.

[23] W. Seemann, "A linear ultrasonic traveling wave motor of the ring type," *Smart Mater. Struct.*, vol. 5, no. 3, pp. 361–368, Jun. 1996.

[24] G. P. L. Thomas, M. A. B. Andrade, J. C. Adamowski, and E. C. N. Silva, "Development of an acoustic levitation linear transportation system based on a ring-type structure," *IEEE Trans. Ultrason., Ferroelect., Freq. Control*, vol. 64, no. 5, pp. 839–846, May 2017.

[25] X. Liu, D. Shi, Y. Civet, and Y. Perriard, "Modelling and optimal design of a ring-type structure for the generation of a traveling wave," in *Proc. Int. Conf. Elect. Mach. Syst.*, 2013, pp. 1286–1291.

[26] G. P. L. Thomas, C. Y. Kiyono, A. G. Neto, and E. C. N. Silva, "Conceptual design of oblong ring vibrators," *J. Vib. Acoust.*, vol. 142, no. 2, Dec. 2019, Art. no. 021001.

Zhaochong Cai received the bachelor's degree in optoelectronic engineering from Beihang University, Beijing, China, in 2017, and the M.Sc. degree in optical engineering from Zhejiang University, Hangzhou, China, in 2020. Since December 2020, he has been working toward the Doctoral degree with Cognitive Robotics (CoR) Department within the 3mE Faculty, TU Delft, Delft, the Netherlands. His research interest is on developing surface haptic devices with active force feedback.

Michaël Wiertlewski (Member IEEE) received the Ph.D. degree on the reproduction of tactile textures from the Université Pierre et Marie Curie, Paris, France, under the auspices of the Commissariat à l'Energie Atomique (CEA-LIST), Fontenay-aux-Roses, France, in 2011. He is currently an Assistant Professor with the Cognitive Robotics Department of the TU Delft, Delft, the Netherlands. In 2012, he joined the Neuroscience and Robotics (NxR) Lab with Northwestern University, Evanston, IL, USA where he studied the physics of ultrasonic friction modulation. From 2015 to 2019, he was CNRS Chargé de Recherche with Aix-Marseille University, Marseille, France. He was the recipient of the Early Career Award from the Technical Committee on Haptics in 2017. His main research interests include the design of tactile interfaces, the physics of skin/surface interaction, and tactile perception.